FIELD PERFORMANCE VALIDATION OF AN ADVANCED UTILITY-SCALE PARABOLIC TROUGH CONCENTRATOR

Andrew McMahan[1], David White[2], Randy Gee[3], and Nolan Viljoen[4]

[1]M.Sc., Vice President, Product Management, SkyFuel, Inc. 18300 West Highway 72, Arvada, CO, 80007 USA.
+1 303-330-0276, Andrew.McMahan@SkyFuel.com
[2]Senior Vice President, Engineering, SkyFuel, Inc., 18300 West Highway 72, Arvada, CO, 80007, USA.
[3]Chief Technology Officer, SkyFuel, Inc., 18300 West Highway 72, Arvada, CO, 80007, USA.
[4]Mechanical Engineer, SkyFuel, Inc., 18300 West Highway 72, Arvada, CO, 80007, USA.

Abstract

SkyFuel has developed a parabolic trough solar concentrator, the SkyTrough®, for utility-scale power generation. This collector underwent an extensive development process culminating in a commercial deployment at the existing SEGS-II solar power plant in Daggett, CA, USA. This paper compares the operating data from the commercial demonstration at the SEGS-II plant with model predictions based on single module-scale tests. The comparison is critical for determining that the collector is ready for use in large commercial projects, and will meet acceptance test requirements after installation. The module-scale test results are shown to be an excellent predictor of field performance; specifically, the performance of a single mirror accurately predicts the field performance of multiple mirrors within a single Solar Collector Assembly, and multiple assemblies plumbed in series. The SEGS-II field performance data precisely matches the SkyTrough single module-scale performance model, with very low variance over several contiguous days of operation.

Keywords: Parabolic Trough, CSP, Performance Modeling, Performance Measurement, Acceptance Testing

1. Introduction and Background

The field performance of complete SkyTrough Solar Collector Assemblies (SCAs) in a commercial demonstration project is validated against single module-scale tests. Accurate characterization and demonstration of field performance is an essential step in successful commercialization of a parabolic trough collector product. This performance validation ultimately provides critical information in the development of acceptance testing procedures; however, the analysis executed and described here is limited to examination of the commercial deployment of SkyTrough SCAs at the existing SEGS-II solar power plant in Daggett, CA, USA. The single module-scale testing performed by the National Renewable Energy Laboratory (NREL) is summarized and extended to create a predictive model for field conditions. Field performance measurements with associated uncertainties are provided. The performance results indicate that the SkyTrough commercial demonstration field data precisely matches the single module-scale performance, with very low variance in a single day and over several contiguous days of operation.

1.1. Site description

The collectors are deployed at the SEGS-II (also known as the Sunray Energy Plant) facility in Daggett, CA, USA. SEGS-II has a nameplate capacity of 30 MWe and is owned and operated by Cogentrix Energy, LLC, headquartered in Charlotte, NC, USA.

SEGS-II was originally developed by the Luz Corporation and came online in 1985. The facility features LS-2 and LS-1 parabolic trough collectors. The primary solar field heat transfer fluid (HTF) is Therminol®VP-1, with a small fraction of Therminol®66 added to reduce the freezing point of the mixture.

1.2. Collector description

Each mirror module in the SkyTrough single-axis linear parabolic concentrating collector has an aperture of 6 m (width) by 13.7 m (length). The standard SCA includes 8 mirror modules for a total of 656 m^2 of net aperture area. The mirror panels are supported by an all-aluminum space frame made from extruded components that are shipped directly to the site and field assembled. Slide-in mirror panels, laminated with ReflecTech® Mirror Film, span the entire aperture width, and are used in place of traditional glass mirror technology. The collector uses Schott PTR®80 4.7m receivers. Collector tracking is powered by a single hydraulic rotary actuator, and controlled with a local microprocessor that calculates sun-position and monitors an inclinometer for feedback on collector position. The local SCA controllers communicate with the power plant supervisory control via an RS-485 connection. Wireless communication is also supported for

supervisory control, though this capability is used only for remote internet monitoring in this deployment. The collector requires no module-to-module or individual mirror panel adjustment in the field. The mirror module-scale tests reliably predict the performance of a complete SCA, and ultimately the performance of a complete field, in part because there are no field adjustments.

1.3. System description

The demonstration at SEGS-II includes three SCAs, two of which have fewer than eight modules to accommodate land restrictions, with a total of 1,500 m^2 in aperture. The system was assembled by an independent EPC contractor, and construction was completed in December, 2009. The entire SEGS-II plant shut down for routine annual maintenance in January 2010, and the demonstration system has operated continuously under plant control since February 2010. Precision instrumentation and a data acquisition system (DAQ) for performance monitoring and validation were installed and calibrated in June, 2010.

The collector system has experienced a wide range of operating conditions: ambient temperatures from -10 to 49°C, operating temperatures from cold start to 315°C (including an HTF freeze event), HTF Pressure from 100 to 1,000 kPa, Direct Normal Insolation (DNI) from 0 to 1050 W/m^2, wind speed from 0 to 27 m/s and a wide variety of weather conditions (sun, rain, thunderstorms, light snow).

1.4. Previous work and commercial relevance

NREL test facilities provided the optical efficiency, incident angle modifier, and receiver loss for a single mirror module that provides the basis for this performance validation (see section 2). Significant prior work in collector performance characterization at the module scale exists, much of it performed on the AZTRAK platform at Sandia National Labs in Albuquerque, NM, USA [1]. The AZTRAK is similar to the NREL facility used in this work, and has the ability to directly measure thermal efficiency at high temperatures. The AZTRAK cannot accommodate large mirror modules; consequently a truncated version of the SkyTrough mirror module is currently installed on the AZTRAK platform. Thermal performance data is being gathered, and the results from AZTRAK will be compared to the results presented here in future work.

As the Concentrating Solar Power (CSP) market grows around the world, commercial interest in performance validation is increasing. Providers of large commercial solar fields and solar collector technology are required to guarantee the performance of their equipment. Standard metrics and corresponding test procedures are needed to verify the performance of a collector field after it is commissioned. Efforts are ongoing through SolarPACES and the American Society of Mechanical Engineers (ASME) to address these needs in a standardized way, but there is currently no consensus in the industry regarding the best approach.

This paper extends module-scale collector testing to a series of SCAs, operating in a commercial environment; an important exercise that has previously been absent from the widely-circulated literature.

2.0. Mirror Module-Scale Testing

Prior to its deployment at SEGS-II, the collector underwent significant testing to determine its performance characteristics. Optical efficiency and incidence angle modifier at the module-scale were measured, and receiver heat loss was characterized in bench-top tests. The results of these tests, along with the approach taken to performance validation in the field, are discussed in this section.

2.1. NREL module-scale optical testing

The collector was tested at the NREL Optical Efficiency Test Loop [2], shown in Figure 1. This test platform circulates a glycol solution at temperatures close to ambient to enable precise measurement of collector optical efficiency and Incidence Angle Modifier (IAM).

Fig. 1. (LEFT) Collector Module Test at NREL and (RIGHT) collector loop at SEGS-II

The optical efficiency at normal incidence was found to be:

$$\eta_0 = 0.773 \qquad (eqn.1)$$

The IAM, without cosine losses, was found to be (where θ_d is the incidence angle expressed in degrees):

$$IAM(\theta_d) = (-3 \cdot 10^{-5}) \cdot \theta_d^2 - 0.0002 \cdot \theta_d + 1 \qquad (eqn.2)$$

2.2 NREL receiver heat loss testing

A Schott PTR80 receiver was tested by NREL in their Receiver Heat Loss Test Facility [3]. These experimental results were combined with the analytical model from [4] to create the following estimate of receiver heat loss:

$$\dot{Q}_{HeatLoss} = A0 + A1 \cdot (T_{HTF} - T_{ambient}) + A2 \cdot {T_{HTF}}^2 + A3 \cdot {T_{HTF}}^3 + A4 \cdot DNI \cdot IAM(\theta) \cdot \cos(\theta) \cdot {T_{HTF}}^2 + \sqrt{V_{wind}} \cdot [A5 + A6 \cdot (T_{HTF} - T_{ambient})] \qquad (eqn.3)$$

A0	A1	A2	A3	A4	A5	A6
6.41	0.308	-1.95E-03	7.29E-06	1.08E-07	-2.89	0.205

Table 1. Receiver Heat Loss Correlation Coefficients

2.3 Field optical characterization

The distant observer method [5] was used to provide a preliminary evaluation of the optics of a complete SCA deployed in the field. This analysis yielded an estimated intercept factor of >99% for the eastern-most collector in the SEGS-II loop. The other collectors in the loop were not tested using this method due to the difficulty in finding a suitable location from which to take photos.

Fig. 2. Distant observer image from SEGS-II demonstration loop showing >99% intercept factor

2.4 Testing objective and approach

The objective of the field testing carried out in this work is to verify that the performance of full-scale collectors operating in a commercial environment is consistent with the performance predicted by module-scale tests. The module-scale test results are used to develop a steady-state collector performance model which calculates net thermal energy collection. The results of the performance model are then compared with the measured thermal energy delivered at the loop outlet. Data is analyzed during the daily period from collector deployment to collector stow.

The data is compared to the performance model both for instantaneous energy collection and total energy collected over multiple operating days. This method quantifies how closely the collector achieves its expected design-point performance (clear-sky, mid-day), as well as total performance over the range of operating conditions and transients experienced on sub-optimal solar days, startup and shut-down.

3.0 Translation of Test Data to Predicted Performance

Combining the optical efficiency (energy gain) and receiver heat loss (energy loss) yields a governing equation for net thermal gain:

$$\dot{Q}_{predicted} = DNI \cdot A \cdot \eta_{modified} - N_{receivers} \cdot L_{receivers} \cdot \dot{Q}_{HeatLoss} \quad (eqn.4)$$

This equation requires incorporation of the NREL module-scale test results and adjustments to those results to account for actual operating conditions. The energy gain term must account for off-normal solar incidence, end losses, shading, receiver modifications, and the cleanliness of the SCA. The energy loss must account for operating temperature.

3.1. Optical efficiency adjustments

The predicted performance requires adjustment to optical efficiency accommodate deviations between test and actual conditions:

$$\eta_{modified} = \eta_0 \cdot IAM \cdot \cos\theta_d \cdot F_{Shield} \cdot F_{EndLoss} \cdot F_{RowShadow} \cdot F_{clean} \qquad (eqn.5)$$

The calculation of η_0 is made at normal incidence, so both IAM losses and cosine losses must be included for normal operation at non-zero incidence. Incidence angle, θ_d, is calculated based on the formulas of Blanco-Muriel, et.al. [6], including corrections for the actual row azimuth which was determined by site survey.

The NREL optical test report provides efficiency for the collector with the PTR®80 receivers with no shielding. Radiation shields were added at the commercial installation, as recommended by Schott Solar (See Figure 3). This shield reduces the active length of the receiver, the effective aperture, and therefore the predicted performance. The distance between bellows defines the active receiver length as tested, and the active length of the commercial receiver is the distance between radiation shields. The net impact on performance is equal to the ratio of active lengths, and varies from 0.964 to 0.961 for receiver temperatures of 25°C and 300°C, respectively. To maintain simplicity, the conservative value of 0.964 is used for F_{Shield}

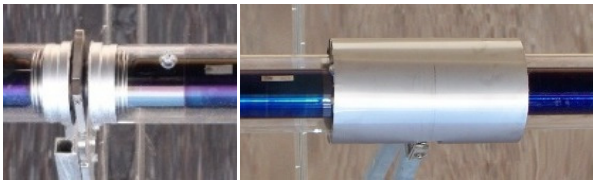

Fig. 3. (LEFT) PTR80 as tested at NREL (RIGHT) PTR80 as installed at SEGS II

In addition to the losses associated with the radiation shield, a portion of the receiver tube is not illuminated at the end of an SCA when the sun is away from normal incidence. The efficiency is decreased by the $F_{EndLoss}$ term as described by Lippke [7], and modified to accommodate losses at the end and drive.

$$F_{EndLoss} = 1 - 2 \cdot \frac{f \cdot tan(\theta_d)}{L_{SCA}} \qquad (eqn.6)$$

$F_{RowShadow}$, accounts for shading by adjacent SCAs in the early morning and late afternoon. The reduction in thermal performance is classically described by Kutscher, et.al. [8]:

$$F_{RowShadow} = \frac{L_{Spacing} \cdot cos(\theta_z)}{W_{aperture} \cdot cos(\theta_d)} \qquad (eqn.7)$$

The demonstration loop is at the eastern edge of the field. Consequently, only one SCA is fully shaded, and a second partially shaded the morning. In the afternoon, all SCAs are shaded; however, two are blocked by the existing LS-2 collectors, with a smaller aperture width. The $F_{RowShadow}$ term is calculated for each SCA separately, with different results in the morning and afternoon.

F_{Clean} represents the loss associated with dirt that accumulates on optical surfaces between cleanings, and is dominated by the reduction in reflectance when the mirror panels are dirty. Reflectance measurements are taken at four positions on each concentrator module (72 total measurements) with a Devices and Services (D&S) Specular Reflectometer at the 25 milliradian acceptance angle position. The wash protocol for this system is high pressure hose down with de-ionized water only. The receivers have never been separately washed since installation in October 2009. The wash period for mirrors varies from no cleaning through winter and spring months to a maximum weekly frequency in summer dependent on plant maintenance activities and weather. Clean specular reflectance for the ReflecTech mirror panels is 94%, and this reflectance value is typically achieved after a wash cycle as shown in Figure 4.2.

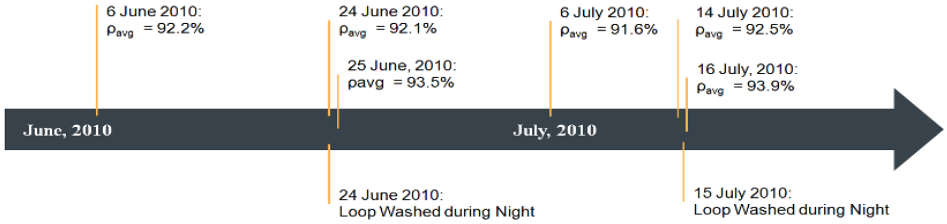

Fig. 4. Reflectance, measured with a D&S Specular Reflectometer at 25 milliradian acceptance angle, varies from 91 to 94%, and is restored after each wash

The performance data presented in subsequent sections of this paper are provided for 19 June through 09 July 2010. The single day output detail is shown for 19 June; the average reflectance is 92.1%, and the ratio of average to clean reflectance is: 0.921 / 0.940 = 0.98. The value selected for F_{Clean}, 0.97, includes an estimated one point reduction to account for the dirt accumulation on the receiver glass.

3.2. Receiver heat loss calculation

Receiver surface temperatures vary both axially (along the length of the collector loop) and radially (around the receivers circular cross-section) during normal operation. Equation 3 includes a term that accounts for the non-uniform radial surface temperature distribution that occurs when the receiver is irradiated. The axial receiver temperature distribution is assumed to be linear[1]:

$$T_{HTF} = \frac{(T_{inlet,^\circ C} + T_{outlet,^\circ C})}{2} \qquad (eqn. 8)$$

3.3. Uncertainty in the predicted performance

Predicted performance requires only two measured values: the mirror reflectance and the DNI. Reflectance measurements are made with a Device & Services specular reflectometer. The DNI measurement is taken with a rotating shadow band radiometer (RSR), and is reported on a five second interval. That radiometer output was manually calibrated against the much more precise U.S. National Institute of Standards and Technology (NIST) traceable Eppley Normal Incidence Pyrheliometer.

The systematic instrument error for reflectance is $\pm$0.1%, and random measurement error is $\pm$0.2%. The systematic DNI instrument error is $\pm$ 2%, and the random measurement uncertainty is $\pm$ 0.13%. The combined total uncertainty in predicted performance, expressed at a 95% confidence level, is 2.1%.

4. Measured Performance and Uncertainty

The thermal performance from measured inputs is defined by the following, classical equation:

$$\dot{Q}_{measured} = \dot{m} \cdot C_p \cdot (T_{outlet} - T_{inlet}) \qquad (eqn. 9)$$

The flow rate and temperature differential, are essentially determined by direct field measurement. Specific heat for the heat transfer fluid (C_p) was established by a series of independent lab measurements. The uncertainties in the field and lab measured values are treated separately in the following sections. The total combined uncertainty in measured performance is 4.0%. *The error is dominated by the uncertainty in specific heat*, a value that is frequently neglected in high temperature performance testing.

The uncertainty (U) for a series of independent errors is classically described by the root sum square (r-s-s) of each term (X_i), and each term is the product of the sensitivity and error. The relationship between the result and measured values is known (eqn. 9), and the sensitivity can be obtained by partial differentiation:

$$U^2 = \sum \left(\frac{\delta \dot{Q}_{measured}}{\delta X_i} \cdot \varepsilon_{X_i} \right)^2 \qquad (eqn. 10)$$

The error term is a combination of systematic error, an uncertainty in the 'true' value associated with the accuracy of an instrument or a fluid property, and the random error associated with standard variance in repeated measurements of a 'true' or mean value. Random error terms are normalized to the mean, and so are expressed as a percentage. The systematic error, and the product of random error and the value of the student's t distribution given the number of measurements and a 95% confidence level, are combined in r-s-s fashion to produce the error term (ε) in equation 10. This procedure is used in all estimates of uncertainty for predicted and measured performance.

4.1. Uncertainty of field measured values

The HTF temperature is directly measured with a Type J precision thermocouple. The thermocouple cold junction compensation is provided by a transmitter that also converts the millivolt output to a milliamp current signal. That transmitter is calibrated against a precision millivolt source at ten points that correspond to a thermocouple output between 100 and 300°C to reduce error associated with non-linear transmitter response. Finally, the transmitter output is read by an analog to digital converter, and data is recorded on a five second interval. The systematic error of each device is independent, and the total accuracy of a single temperature measurement is the r-s-s of the accuracy for the thermocouple, transmitter, and analog to digital (A to D) converter.

The random error for T_{inlet} and T_{outlet} was determined empirically. Data measurements were examined near solar noon, after the system operation had reached steady state conditions for approximately one hour. The

[1] The temperature distribution along the loop is not perfectly linear, but the calculation of $Q_{predicted}$ is extremely insensitive to this assumption so no attempt to refine it was made.

data set was reduced to individual measurements where the DNI and flow rate were virtually constant, and the standard deviation of the subsequent temperature data defines the random error. The student's t distribution for the reduced data set yields a value of 1.98 for a 95% confidence level.

The HTF volumetric flow rate is directly measured with an orifice plate and differential pressure transmitter. The transmitter is furnished with an NIST-traceable calibration certificate. Like temperature, the transmitter output is read by an analog to digital converter, and data is recorded on a five second interval. The systematic error of each device is independent, and the total accuracy of a single volumetric flow rate measurement is the r-s-s of the accuracy for the orifice plate (coefficient of discharge), transmitter, and A to D converter.

The random error in volumetric flow rate was determined empirically, similar to the procedure described for temperature, except the data set was reduced to individual measurements where the DNI and inlet temperature were virtually constant. The number of measurements in the reduced data set for flow is identical to the count in temperature; consequently, the student's t distribution also yields a value of 1.98.

The product of fluid density and volumetric flow rate yields the mass flow rate, the variable used to define thermal performance (eqn. 9). Fluid density was defined by independent lab tests, the uncertainty of the result is smaller by an order of magnitude than the systematic or random error in flow, and uncertainty in density is neglected; however, *the fluid density is a function of temperature*. *The specific heat fluid property is also a function of temperature.* Consequently, the random uncertainty in temperature measurements propagates to both mass flow rate and specific heat.

Fluid properties were established by independent laboratory tests, and a regression analysis provides the relationships for density in kg/m^3 and specific heat in kJ/kg-°C, respectively:

$$\rho = 1061.5 - 0.6701 \cdot T_{inlet} \quad (eqn.\,11) \qquad C_p = 1.5174 + 0.0025 \cdot \left(\frac{T_{inlet}+T_{outlet}}{2}\right) \quad (eqn.\,12)$$

Equations 11 and 12 are substituted into equation 9 to create a relationship for the measured performance that is a function of temperature and volumetric flow rate only. Partial differentiation of that relationship with respect to T_{inlet}, T_{outlet}, and volumetric flow rate provides the sensitivity of each term. There is no propagation of error associated with flow rate.

Measured value	Sensitivity	Systematic ε	Random σ	Student t	Random ε	Combined ε
T_{inlet}	-2.2% per%	0.424%	0.223%	1.98	0.441%	1.37%
T_{outlet}	+3.3% per%	0.424%	0.119%	1.98	0.376%	1.60%
Volumetric Flow	+1.0% per%	1.256%	0.290%	1.98	0.574%	1.38%
Combined Instrument Uncertainty, with a 95% Confidence Level						2.52%

Table 2. Uncertainty in measured performance for the field instrumentation

4.2. Uncertainty in fluid properties

The key fluid properties of density and specific heat affect performance measurements. The properties were established by independent testing laboratories. Density was measured from 25 to 200°C using simple procedures and NIST-traceable instruments. The results are assumed to be precise and without bias. The specific heat is substantially more difficult to measure, and the resultant uncertainties are considerable compared to the field instrument measurements.

Specific heat was established with Differential Scanning Calorimetry in accordance with the ASTM E-1269 standard. Eighteen distinct test series were executed between 20 and 220°C at 5°C intervals. The response was nearly linear over the temperature range for all tests, and the rate of change in specific heat with respect to temperature was relatively constant. Mean values were within 1% of catalog data, suggesting that the fluid has not degraded, and Cogentrix/Sunray properly maintains the HTF. The uncertainty in the results, however, remains significant: 3.1% expressed at a 95% confidence level. The combined uncertainty, including both specific heat and field measurements, increases to 4.0% of measured thermal performance at the 95% confidence level when the fundamental uncertainty of the specific heat fluid property is included.

While low temperature testing that establishes the optical efficiency of the collector incorporates specific heat measurements with a small uncertainty [2], high temperature performance testing by the national laboratories typically ignore the fundamental uncertainty in specific heat [1], and limit reporting to the measured temperature error propagation described in the previous section. The uncertainty in specific heat measured during this field verification is larger than instrument error, and substantially larger than the instrument errors typically used in independent module performance testing. No independent laboratories were identified that

are capable of testing reliably at higher temperatures (above the boiling point of Therminol®VP-1 at ambient pressure), and the fluid manufacturer acknowledged that catalog data is based on similar testing procedures and has uncertainties that are not reported [9]. Consequently, the national labs might consider adding verification specific heat measurement capabilities at higher operating temperatures to refine estimates of uncertainty in performance tests. Accurate examination of this heat transfer fluid property would also be beneficial during acceptance testing for CSP plants.

5. Performance Results and Validation

The instantaneous daily predicted performance (kW-th), measured performance (kW-th), and DNI data (W/m^2) for 19 June 2010 is shown in Figure 5. Dual error bars illustrate instrument uncertainty, and combined instrument and specific heat uncertainty. The measured and predicted performances are virtually identical for the majority of the day, and depart from one another under non-steady state conditions. A control peculiarity is reflected by performance in the very early morning: the collectors are deployed near 5:40AM local standard time to a fixed position and do not begin to track until 6:00 AM. This operational peculiarity accommodates light level requirements for optical trackers on existing LS2 collectors, and is not required for the SkyTrough. Performance between 6:00 and 7:00AM falls below predictions, likely due to cold receivers, cold fluid in the receivers, and cold fluid slugs from the header on the first passes through the plant. Late afternoon performance shows the opposite trend: measured performance exceeds predicted values likely due to the slow reduction in supply temperatures, and the thermal inertia associated with the receivers and fluid.

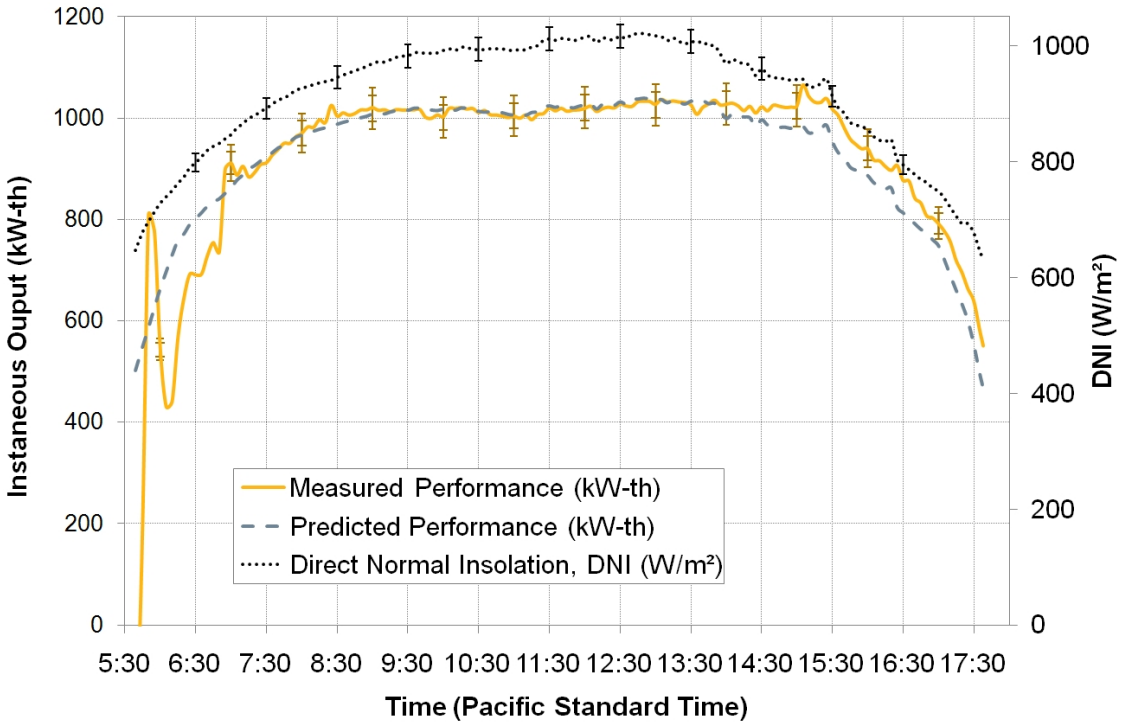

Fig. 5. Predicted and Measured Performance, with DNI data, for a complete day

The instantaneous performance is integrated each day from the early morning deploy to late afternoon stow signals. Figure 6 shows integrated DNI and performance values (kWhr / day) for twenty one contiguous days between 19 June and 9 July, 2010. The periods with reduced integrated DNI and performance reflect service withdrawals associated with instrument calibration, partially cloudy days, and stow for approximately eight hours while local wind speeds exceeded 22.5 m/s. The ratio of measured to predicted thermal performance is also shown on the chart, and the twenty one days exhibit a mean ratio of 100.1%, a standard deviation less than 1.6%, and a combined uncertainty less than 5% for a 95% confidence level.

The measured field performance of this collector, implemented in a commercial facility, precisely matches the performance predictions based on NREL single module-scale concentrator and receiver testing. This trend is demonstrated in single day measurements, as well as integrated performance over several contiguous days with very low variance.

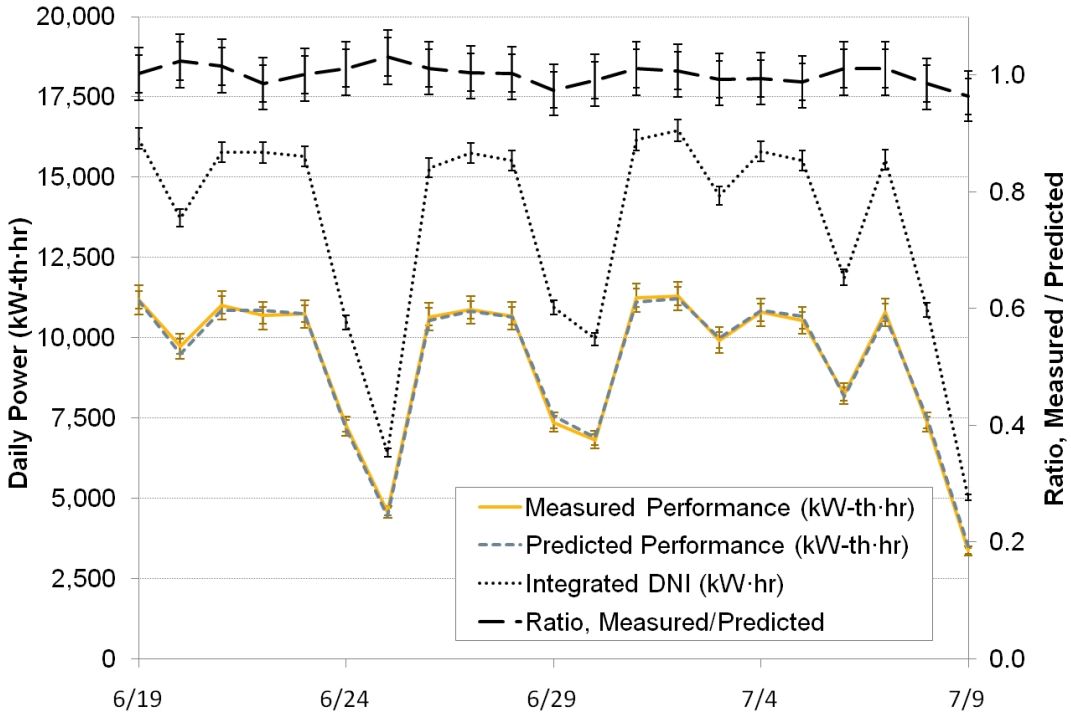

Fig. 6. Integrated Performance, with DNI data, for several contiguous days

6. Conclusions

The SkyTrough collector system studied in this paper has demonstrated performance in the field for complete SCAs that is accurately predicted by the single module tests performed by NREL. This result provides validation that the performance of this collector system successfully scales from the test stand to the field and from the module-scale to the SCA-scale. It further demonstrates that the module-scale tests provide a sufficient basis for developing field performance models of well designed parabolic trough solar concentrators.

Acknowledgements

This work would not have been possible without the support of Cogentrix Energy LLC. that provided a site for the demonstration facility at SEGS-II in Daggett, CA, USA, and the National Renewable Energy Laboratory (NREL), that performed the scale optical efficiency and receiver heat loss tests.

References

[1] Dudley, V.E., et al, (1994). Test Results: SEGS LS-2 Solar Collector. Sandia National Laboratories Report, SAND94-1884, Albuquerque, NM

[2] Gawlik, K., Stynes, K., Kutscher, C., (2010). Optical Efficiency Measurements of the SkyTrough Solar Collector. National Renewable Energy Laboratory Preliminary Publication, Golden, CO

[3] Crawford, J., Burkholder, F., (2009). Heat Loss Testing of Schott's Prototype PTR 80-4.7 (2008) Parabolic Trough Receiver. National Renewable Energy Laboratory Preliminary Publication, Golden, CO

[4] Forristall, R., (2003). Heat Transfer Analysis and Modeling of a Parabolic Trough Solar Receiver Implemented in Engineering Equation Solver. National Renewable Energy Laboratory Technical Report, NREL/TP-550-34169, Golden, CO

[5] Diver, R.B., Moss, T.A., *Practical Field Alignment of Parabolic Trough Solar Concentrators*. ASME Journal of Solar Energy Engineering, 129 (2007) 153-159

[6] Blanco-Muriel, M., et al., *Computing The Solar Vector*. Solar Energy, 70(5) (2001) 431-441

[7] Lippke, F., (1995). Simulation of the Part Load Behavior of a 30MWe SEGS Plant. Sandia National Laboratories Report, SAND95-1293, Albuquerque, NM

[8] Kutscher, C.F., Davenport, R.L., Dougherty, D.A., Gee, R.C., Masterson, P.M.; May, E.K. (1982) Design Approaches for Solar Industrial Process Heat Systems. Solar Energy Research Institute, SERI TR/253-1356

[9] E-mail communication with Solutia, Inc.